

Homology-based Distributed Coverage Hole Detection in Wireless Sensor Networks

Feng Yan, Anaïs Vergne, Philippe Martins, *Senior Member, IEEE*, Laurent Decreasefond

Abstract—Homology theory provides new and powerful solutions to address the coverage problems in wireless sensor networks (WSNs). They are based on algebraic objects, such as Čech complex and Rips complex. Čech complex gives accurate information about coverage quality but requires a precise knowledge of the relative locations of nodes. This assumption is rather strong and hard to implement in practical deployments. Rips complex provides an approximation of Čech complex. It is easier to build and does not require any knowledge of nodes location. This simplicity is at the expense of accuracy. Rips complex can not always detect all coverage holes. It is then necessary to evaluate its accuracy. This work proposes to use the proportion of the area of undiscovered coverage holes as performance criteria. Investigations show that it depends on the ratio between communication and sensing radii of a sensor. Closed-form expressions for lower and upper bounds of the accuracy are also derived. For those coverage holes which can be discovered by Rips complex, a homology-based distributed algorithm is proposed to detect them. Simulation results are consistent with the proposed analytical lower bound, with a maximum difference of 0.5%. Upper bound performance depends on the ratio of communication and sensing radii. Simulations also show that the algorithm can localize about 99% coverage holes in about 99% cases.

Index Terms—Wireless sensor networks, coverage hole, homology.

I. INTRODUCTION

WIRELESS sensor networks (WSNs) have attracted a great deal of research attention due to their wide potential applications such as battlefield surveillance, environmental monitoring and intrusion detection. Many of these applications require a reliable detection of specified events. Such requirement can be guaranteed only if the target field monitored by a WSN contains no coverage holes, that is to say regions of the domain not monitored by any sensor. Coverage holes can be formed for many reasons, such as random deployment, energy depletion or destruction of sensors. Consequently, it is essential to detect and localize coverage holes in order to ensure the full operability of a WSN.

There is already an extensive literature about the coverage problems in WSNs. Several approaches are based on computational geometry with tools such as Voronoi diagram and Delaunay triangulations, to discover coverage holes [1]–[3]. These methods require precise information about sensor locations. This substantially limits their applicability since acquiring accurate location information is either expensive or impractical in many settings. Some other approaches attempt to discover coverage holes by using only relative distances

between neighbouring sensors [4]–[6]. Similarly, obtaining precise range between neighbour nodes is costly.

More recently, homology is utilized in [7]–[9] to address the coverage problems in WSNs. Ghrist and his collaborators introduced a combinatorial object, Čech complex (also known as nerve complex), which fully characterizes coverage properties of a WSN (existence and locations of holes). Unfortunately, this object is very difficult to construct as it requires rather precise information about the relative locations of sensors. Thus, they introduced a more easily computable complex, Rips complex (also known as Vietoris-Rips complex). This complex is constructed with the sole knowledge of the connectivity graph of the network and gives an approximate coverage by simple algebraic calculations. As regards implementation in real WSN, these homology based methods are necessarily centralized, which makes them impractical in large scale sensor networks. Some algorithms have been proposed to implement the above mentioned ideas in a distributed context, see [10], [11]. But there are two disadvantages of these algorithms. On one hand, these homology based algorithms are all dependent on the assumption that the communication radius of a sensor is smaller than $\sqrt{3}$ times the sensing radius of the sensor. When such assumption is not satisfied, it is possible that Rips complex may miss some special coverage holes (such holes are defined as triangular holes in Section III). It is thus of paramount importance to determine the proportion of missed coverage holes to assess the accuracy of Rips complex based coverage hole detection. On the other hand, these algorithms are either slow or require coverage holes separated with enough distance. So it is necessary to design an efficient and accurate algorithm to detect coverage holes.

The main contributions of our paper are as follows. First, The relationship between Čech complex and Rips complex in terms of coverage hole is analysed under different ratios between communication and sensing radii of a sensor. We find that when the communication radius is at least two times sensing radius, if there is a hole in Rips complex, there must be a hole in Čech complex. A hole in a Čech complex missed by a Rips complex must be bounded by a triangle. Based on that, a formal definition of triangular and non-triangular hole is presented.

Second, the proportion of the area of triangular holes under a homogeneous setting is analysed. It is indicated that such proportion is related to the ratio between communication and sensing radii of each sensor. In addition, closed-form expressions for lower and upper bounds of the proportion under different ratios between communication and sensing

F. Yan, A. Vergne, P. Martins and L. Decreasefond are with the Network and Computer Science Department, TELECOM ParisTech, Paris, France.

radii are derived.

Third, a homology based distributed algorithm is proposed to detect non-triangular coverage holes. In the algorithm, a Rips complex is first constructed for a given WSN. Then some vertices and edges are deleted without changing the number of holes in the original Rips complex. After that, the edges lying on the boundary of holes will be detected. Then coarse boundary cycles can be discovered. Finally all boundaries of the non-triangular holes are found by minimizing the length of coarse boundary cycles.

The remainder of the paper is organized as follows. Section II presents the related work. In Section III, the network model and the formal definition of triangular and non-triangular hole are given. Upper and lower bounds on the proportion of the area of triangular holes under different ratios between communication and sensing radii are computed in Section IV. Section V describes the homology based distributed algorithm for non-triangular holes detection. In Section VI, performance evaluation of the bounds and the algorithm is given. Finally, Section VII concludes the paper.

II. RELATED WORK

There is not much work on the proportion of the area of triangular holes. Some recent work [12]–[15] provides some results on coverage probability but with a different point of view. In [12], [13], the fraction of the area covered by sensors is analysed. In [14], the authors study how the probability of coverage changes with the sensing radius or the number of sensors. In [15], a point in a plane is defined to be tri-covered if it lies inside a triangle formed by three nodes, and the probability of tri-coverage is analysed. None of them considers triangular holes, we provide some initial results about proportion of triangular holes in [16].

The related work on the coverage problem in WSNs can be generally classified into three categories: location-based, range-based and connectivity-based. In the first category, the Voronoi diagram is used to detect boundary nodes in [1], [2]. In [3], a boundary node detection algorithm based on localized Voronoi polygons is proposed. In [17], it is proved that a sensor node does not border a coverage hole if its sensing border is entirely covered by the sensing ranges of its neighbours. Another boundary node detection approach proposed in [18] simplifies the previous border-checking approach by only checking intersection points on the sensing border. The former algorithms only detect boundary nodes but do not detect boundary cycles. Based on that, the authors propose a method to obtain the exact boundary cycles of coverage holes in [19].

Range-based approaches attempt to identify boundary nodes based on relative distance between neighbouring nodes. In [4], a localized Voronoi polygon based boundary node detection algorithm is proposed, which is similar as that in [3]. The difference lies in that the localized Voronoi polygon is constructed using location information of nodes in [3] while it is constructed based on directional and distance information between neighbouring nodes in [4]. In [5], [6], the author proposes a coverage verification algorithm based on

distances between neighbouring nodes. These approaches also only detect boundary nodes without discovering all boundary cycles.

Connectivity-based schemes try to discover boundary cycles using only connectivity information. Our algorithm belongs to this category. As a pioneer work, in [7], Ghrist et al propose an algorithm that detects coverage holes via homology. They construct the Rips complex corresponding to the communication graph of the network and determine the coverage by verifying whether the first homology group of the Rips complex is trivial. But their method is centralized. The first steps of implementing the above ideas in a distributed way are taken in [10]. It is shown that combinatorial Laplacians are the right tools for distributed computation of homology groups and can be used for decentralized coverage verification. In [20], a gossip-like decentralized algorithm for computation of homology groups is proposed. But its convergence is slow. In [11], a decentralized scheme based on Laplacian flows is proposed to compute a generator of the first homology. And they formulate the problem of localizing coverage holes as an optimization problem for computing a sparse generator of the first homology. But it is possible that some cycle found by their algorithm encircles more than one coverage holes. More recently, some distributed algorithms are proposed to detect topological holes [21], [22] and some other algorithms are proposed for boundary recognition in sensor networks by using only connectivity information [23]–[26]. These algorithms may be useful for coverage hole detection, but they can only detect large coverage holes and may miss small area coverage holes. The algorithm proposed in [27] can detect all non-triangular holes, but our algorithm is more efficient, especially when coverage holes are largely separated.

III. MODELS AND DEFINITIONS

A brief introduction to the tools used in the paper is given. For further readings, see [28]–[30]. Given a set of points V , a k -simplex is an unordered set $[v_0, v_1, \dots, v_k] \subseteq V$ where $v_i \neq v_j$ for all $i \neq j$. So a 0-simplex is a vertex, a 1-simplex is an edge and a 2-simplex is a triangle with its interior included, see Figure 1. In the following part, a triangle refers to a 2-simplex if not indicated explicitly. The faces of this k -simplex consist of all $(k-1)$ -simplex of the form $[v_0, \dots, v_{i-1}, v_{i+1}, \dots, v_k]$ for $0 \leq i \leq k$. A simplicial complex is a collection of simplices which is closed with respect to inclusion of faces.

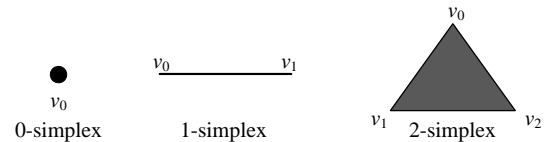


Fig. 1. 0-, 1- and 2-simplex

Čech complex and Rips complex are two simplicial complexes defined as follows [9].

Definition 1 (Čech complex). *Given a collection of sets \mathcal{U} , Čech complex of \mathcal{U} , $\check{C}(\mathcal{U})$, is the abstract simplicial complex*

whose k -simplices correspond to non-empty intersections of $k + 1$ distinct elements of \mathcal{U} .

Definition 2 (Rips complex). *Given a set of points \mathcal{X} in \mathbb{R}^n and a fixed radius ϵ , the Rips complex of \mathcal{X} , $\mathcal{R}_\epsilon(\mathcal{X})$, is the abstract simplicial complex whose k -simplices correspond to unordered $(k + 1)$ -tuples of points in \mathcal{X} which are pairwise within Euclidean distance ϵ of each other.*

Consider a collection of stationary sensors (also called nodes) deployed randomly in a planar target field. As usual, isotropic radio propagation is assumed. Each sensor monitors a region within a circle of radius R_s and may communicate with other sensors within a circle of radius R_c .

In addition, some other assumptions are as follows.

- 1) There are sensors located on the external boundary of the target field. They are known as fence sensors and other sensors are referred to as internal sensors. Each fence sensor has two fence neighbours. This is also the general assumption in many homology based algorithms [7]–[9], [11].
- 2) Although sensors are not aware of their locations, every sensor can know whether it is a fence or an internal node by using the mechanisms presented in [5] or other methods as in [25]. In fact, it is a conventional assumption adopted by many existing range-based methods [5], [31] or connectivity methods [11], [25].
- 3) Internal sensors are distributed in the planar target field according to a homogeneous Poisson point process with intensity λ .
- 4) Each sensor has a unique ID.
- 5) The network has only one connected component.

Let \mathcal{V} denote the set of sensor locations in a WSN and $\mathcal{S} = \{s_v, v \in \mathcal{V}\}$ denote the collection of sensing ranges of these sensors. For a location v , $s_v = \{x \in \mathbb{R}^2 : \|x - v\| \leq R_s\}$. Then, according to the definition, the Čech complex and Rips complex of the WSN, respectively denoted by $\check{C}_{R_s}(\mathcal{V})$ and $\mathcal{R}_{R_c}(\mathcal{V})$, can be constructed as follows: a k -simplex $[v_0, v_1, \dots, v_k]$ belongs to $\check{C}_{R_s}(\mathcal{V})$ whenever $\bigcap_{i=0}^k s_{v_i} \neq \emptyset$ and a k -simplex $[v_0, v_1, \dots, v_k]$ belongs to $\mathcal{R}_{R_c}(\mathcal{V})$ whenever $\|v_l - v_m\| \leq R_c$ for all $0 \leq l < m \leq k$.

Figure 2 shows a WSN, its Čech complex and two Rips complexes for two different values of R_c . Depending on the ratio R_c over R_s , the Rips complex and the Čech complex may be close or rather different. In this example, for $R_c = 2R_s$, the Rips complex sees the hole surrounded by 2, 3, 5, 6 as in the Čech complex whereas it is missed in the Rips complex for $R_c = 2.5R_s$. At the same time, the true coverage hole surrounded by 1, 2, 6 is missed in both Rips complexes.

In fact, as proved in [7], any coverage hole can be found in Čech complex. Furthermore, there are following relations between Čech complex and Rips complex:

$$\mathcal{R}_{R_c}(\mathcal{V}) \subset \check{C}_{R_s}(\mathcal{V}) \subset \mathcal{R}_{2R_s}(\mathcal{V}), \text{ if } R_c \leq \sqrt{3}R_s. \quad (1)$$

According to (1), some relationships between Čech complex and Rips complex in terms of coverage hole can be derived as illustrated in the following corollaries. For convenience, define $\gamma = R_c/R_s$.

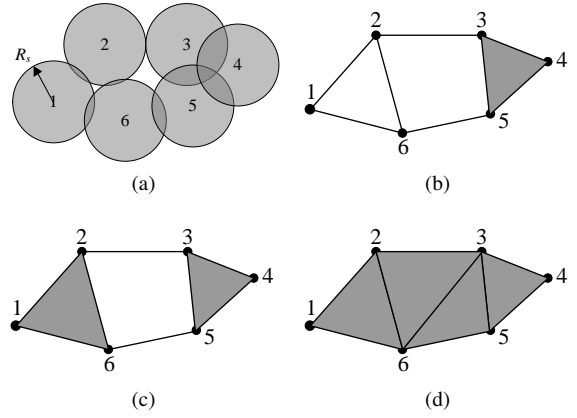


Fig. 2. (a) a WSN, (b) Čech complex, (c) Rips Complex under $R_c = 2R_s$, (d) Rips Complex under $R_c = 2.5R_s$

Corollary 1. *When $\gamma \leq \sqrt{3}$, if there is no hole in Rips complex $\mathcal{R}_{R_c}(\mathcal{V})$, there must be no hole in Čech complex $\check{C}_{R_s}(\mathcal{V})$.*

Proof: If there is no hole in $\mathcal{R}_{R_c}(\mathcal{V})$, it means that $\mathcal{R}_{R_c}(\mathcal{V})$ can be triangulated. Since $\gamma \leq \sqrt{3}$ means $R_c \leq \sqrt{3}R_s$, according to the first inclusion in (1), we can see that $\mathcal{R}_{R_c}(\mathcal{V}) \subset \check{C}_{R_s}(\mathcal{V})$. Consequently, Čech complex $\check{C}_{R_s}(\mathcal{V})$ can also be triangulated. And when $R_c \leq \sqrt{3}R_s$, each triangle must be covered by the sensing range of its vertex nodes [7]. So there is no hole in $\check{C}_{R_s}(\mathcal{V})$. ■

Corollary 2. *When $\gamma \geq 2$, if there is a hole in Rips complex $\mathcal{R}_{R_c}(\mathcal{V})$, there must be a hole in Čech complex $\check{C}_{R_s}(\mathcal{V})$.*

Proof: If there is a hole in $\mathcal{R}_{R_c}(\mathcal{V})$, there must be a cycle with more than three edges in $\mathcal{R}_{R_c}(\mathcal{V})$ that can not be triangulated, as the cycle $\{2, 3, 5, 6\}$ in Figure 2(c). Since $\gamma \geq 2$ means $R_c \geq 2R_s$, according to the second inclusion in (1), we can see that $\check{C}_{R_s}(\mathcal{V}) \subset \mathcal{R}_{2R_s}(\mathcal{V}) \subset \mathcal{R}_{R_c}(\mathcal{V})$. Consequently, there must also be a cycle in $\check{C}_{R_s}(\mathcal{V})$ which can not be triangulated. And there is a coverage hole in the cycle. ■

Corollary 3. *When $\sqrt{3} < \gamma < 2$, there is no guarantee relation between Rips complex $\mathcal{R}_{R_c}(\mathcal{V})$ and Čech complex $\check{C}_{R_s}(\mathcal{V})$ in terms of holes.*

Proof: It is a direct corollary from Corollary 1 and 2. ■

From the discussion above, a hole in a Čech complex not seen in a Rips complex must be bounded by a triangle. Based on this observation, a formal definition of 'triangular hole' and 'non-triangular hole' is given as follows.

Definition 3 (Triangular and non-triangular hole). *For a pair of complexes $\check{C}_{R_s}(\mathcal{V})$ and $\mathcal{R}_{R_c}(\mathcal{V})$, a triangular hole is an uncovered region bounded by a triangle which appears in $\mathcal{R}_{R_c}(\mathcal{V})$ but not in $\check{C}_{R_s}(\mathcal{V})$. Any other holes are non-triangular.*

For triangular holes, it is impossible to detect them with only connectivity information, so we want to analyse the proportion of the area of such holes in a target field. For non-triangular holes, we aim to design a distributed algorithm to discover the boundaries of these holes.

IV. BOUNDS ON PROPORTION OF THE AREA OF TRIANGULAR HOLES

In this section, the conditions under which any point in the target field is inside a triangular hole are first given. From the discussion in Section III, it is found that the proportion of the area of triangular holes is related to the ratio γ . Three different cases are considered for the proportion computation. For each case, the upper and lower bounds of the proportion are derived.

A. Preliminary

Lemma 1. *For any point in the target field, it is inside a triangular hole if and only if the following two conditions are satisfied:*

- 1) *the distance between the point and its closest node is larger than R_s .*
- 2) *the point is inside a triangle: the convex hull of three nodes, two by two less than or equal to R_c apart.*

Lemma 2. *If there exists a point O which is inside a triangular hole, then $R_s < R_c/\sqrt{3}$.*

Proof: According to the definition of triangular holes, if there exists a triangular hole, then there must be a triangle Δ satisfying $\Delta \in \mathcal{R}_{R_c}(\mathcal{V})$ and $\Delta \notin \check{\mathcal{C}}_{R_s}(\mathcal{V})$. If $R_s \geq R_c/\sqrt{3}$, then according to the first inclusion in (1), we have $\mathcal{R}_{R_c}(\mathcal{V}) \in \check{\mathcal{C}}_{R_s}(\mathcal{V})$, it means that there exists not a triangle which is in $\mathcal{R}_{R_c}(\mathcal{V})$ but not in $\check{\mathcal{C}}_{R_s}(\mathcal{V})$, there is a contradiction, so $R_s < R_c/\sqrt{3}$. ■

Lemma 3. *Let O be a point inside a triangular hole and l denote the distance between O and its closest neighbour, then $R_s < l \leq R_c/\sqrt{3}$.*

Proof: $R_s < l$ is a direct corollary from Lemma 1. We only need to prove $l \leq R_c/\sqrt{3}$. If point O is inside a triangular hole, it must be surrounded by a triangle formed by sensors with pairwise distance less than or equal to R_c . Assume it is surrounded by a triangle $N_0N_1N_2$, as in Figure 3. The closest neighbour of O is not necessarily in the set $\{N_0, N_1, N_2\}$. If $l > R_c/\sqrt{3}$, then $d_0 \geq l > R_c/\sqrt{3}$, $d_1 \geq l > R_c/\sqrt{3}$ and $d_2 \geq l > R_c/\sqrt{3}$. In addition, since $\angle N_0ON_1 + \angle N_1ON_2 + \angle N_0ON_2 = 2\pi$, there must be one angle no smaller than $2\pi/3$. Assume $\angle N_0ON_2 \geq 2\pi/3$ and denote it as α . Then according to the law of cosines, $d_{02}^2 = d_0^2 + d_2^2 - 2d_0d_2 \cos \alpha > R_c^2/3 + R_c^2/3 - 2/3R_cR_c \cos(2\pi/3) = R_c^2$. So $d_{02} > R_c$. Since N_0 and N_2 are neighbours, $d_{02} \leq R_c$. There is a contradiction. Therefore $l \leq R_c/\sqrt{3}$. ■

A Poisson point process whose intensity is proportional to the Lebesgue measure is stationary in the sense that any translation of its atoms by a fixed vector does not change its law. Thus without considering border effect [32], any point has the same probability to be inside a triangular hole as the origin O . This probability in a homogeneous setting is also equal to the proportion of the area of triangular holes. We borrow part of the line of proof from [15] where a similar problem is analysed.

We consider the probability that the origin O is inside a triangular hole. Since the length of each edge in the Rips

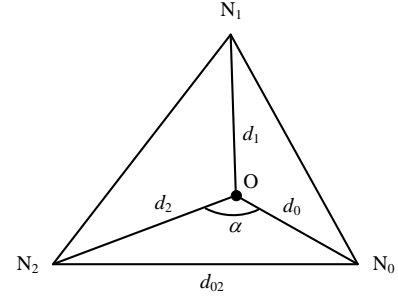


Fig. 3. Illustration of O being inside a triangular hole

complex must be at most R_c , only the nodes within R_c from the origin can contribute to the triangle which bounds a triangular hole containing the origin. Therefore, we only need to consider the Poisson process constrained in the closed ball $B(O, R_c)$ which is also a homogeneous Poisson process with intensity λ . We denote this process as Φ . In addition, $T(x, y, z)$ denotes the property that three points x, y, z are within pairwise Euclidean distance R_c from each other, and the origin O is inside the triangular hole bounded by the triangle with these points as vertices. When n_0, n_1, n_2 are points of the process Φ , $T(n_0, n_1, n_2)$ is also used to denote the event that the triangle formed by the nodes n_0, n_1, n_2 bounds a triangular hole containing the origin. In addition, we use $T'(n_0, n_1, n_2)$ to denote the event that the nodes n_0, n_1, n_2 can not form a triangle which bounds a triangular hole containing the origin.

Let $\tau_0 = \tau_0(\Phi)$ be the node in the process Φ which is closest to the origin. There are two cases for the origin to be inside a triangular hole. The first case is that the node τ_0 can contribute to a triangle which bounds a triangular hole containing the origin. The second case is that the node τ_0 can not contribute to any triangle which bounds a triangular hole containing the origin but other three nodes can form a triangle which bounds a triangular hole containing the origin. So the probability that the origin is inside a triangular hole can be defined as

$$\begin{aligned}
 p(\lambda, \gamma) &= \text{P}\{O \text{ is inside a triangular hole}\} \\
 &= \text{P}\left\{ \bigcup_{\{n_0, n_1, n_2\} \subseteq \Phi} T(n_0, n_1, n_2) \right\} \\
 &= \text{P}\left\{ \bigcup_{\{n_1, n_2\} \subseteq \Phi \setminus \{\tau_0(\Phi)\}} T(\tau_0, n_1, n_2) \right\} \\
 &\quad + \text{P}\left\{ \bigcup_{\{n_0, \dots, n_4\} \subseteq \Phi \setminus \{\tau_0(\Phi)\}} T(n_0, n_1, n_2) \mid T'(\tau_0, n_3, n_4) \right\}
 \end{aligned} \tag{2}$$

In the following parts, we will analyse this probability in three different cases.

B. Case $0 < \gamma \leq \sqrt{3}$

Theorem 1. *When $0 < \gamma \leq \sqrt{3}$, $p(\lambda, \gamma) = 0$.*

Proof: It is a direct corollary from Lemma 2. ■

C. Case $\sqrt{3} < \gamma \leq 2$

Theorem 2. When $\sqrt{3} < \gamma \leq 2$, $p_l(\lambda, \gamma) < p(\lambda, \gamma) < p_u(\lambda, \gamma)$, where

$$p_l(\lambda, \gamma) = 2\pi\lambda^2 \int_{R_s}^{R_c/\sqrt{3}} r_0 dr_0 \int_{\alpha_0}^{\alpha_1} d\theta_1 \int_{r_0}^{R_1(r_0, \theta_1)} e^{-\lambda\pi r_0^2} \times e^{-\lambda|S^+(r_0, \theta_1)|} (1 - e^{-\lambda|S^-(r_0, r_1, \theta_1)|}) r_1 dr_1 \quad (3)$$

and

$$p_u(\lambda, \gamma) = 2\pi\lambda^2 \int_{R_s}^{R_c/\sqrt{3}} r_0 dr_0 \int_{\alpha_0}^{\alpha_1} d\theta_1 \int_{r_0}^{R_1(r_0, \theta_1)} e^{-\lambda\pi r_0^2} \times e^{-\lambda|S^+(r_0, \theta_1)|} (1 - e^{-\lambda|S^-(r_0, r_0, \theta_1)|}) r_1 dr_1 + P\left\{ \bigcup_{\{n_0, \dots, n_4\} \subseteq \Phi \setminus \{\tau_0(\Phi)\}} T(n_0, n_1, n_2) \mid T'(n_0, n_3, n_4) \right\} \quad (4)$$

and

$$\alpha_0 = 2 \arccos(R_c/(2r_0))$$

$$\alpha_1 = 2 \arcsin(R_c/(2r_0)) - 2 \arccos(R_c/(2r_0))$$

$$R_1(r_0, \theta_1) = \min\left(\sqrt{R_c^2 - r_0^2 \sin^2 \theta_1} - r_0 \cos \theta_1, \sqrt{R_c^2 - r_0^2 \sin^2(\theta_1 + \alpha_0)} + r_0 \cos(\theta_1 + \alpha_0)\right)$$

Proof: We first prove the lower bound. It can be obtained from (2) that

$$p(\lambda, \gamma) > P\left\{ \bigcup_{\{n_1, n_2\} \subseteq \Phi \setminus \{\tau_0(\Phi)\}} T(\tau_0, n_1, n_2) \right\}$$

So for the lower bound, we only consider the case that the closest node τ_0 must contribute to a triangle which bounds a triangular hole containing the origin.

Using polar coordinates, we assume the closest node τ_0 lies on (d_0, π) . It is well known that the distance d_0 is a random variable with distribution

$$F_{d_0}(r_0) = P\{d_0 \leq r_0\} = 1 - e^{-\lambda\pi r_0^2} \quad (5)$$

Therefore the above probability can be written as

$$P\left\{ \bigcup_{\{n_1, n_2\} \subseteq \Phi \setminus \{\tau_0(\Phi)\}} T(\tau_0, n_1, n_2) \right\} = \int P\left\{ \bigcup_{\{n_1, n_2\} \subseteq \Phi'_{\tau_0}} T((r_0, \pi), n_1, n_2) \right\} F_{d_0}(dr_0) \quad (6)$$

where Φ'_{τ_0} is the restriction of Φ in $B(O, R_c) \setminus B(O, r_0)$.

Once the node τ_0 is determined, the other two nodes must lie in the different half spaces: one in $H^+ = \mathbb{R}^+ \times (0, \pi)$ and the other in $H^- = \mathbb{R}^+ \times (-\pi, 0)$. Assume n_1 lies in H^+ and n_2 lies in H^- . Since the distance to τ_0 is at most R_c , n_1 and n_2 must also lie in the ball $B(\tau_0, R_c)$. Furthermore, the distance to the origin is at most R_c and larger than d_0 , they should also lie in the area $B(O, R_c) \setminus B(O, d_0)$. Therefore, n_1 must lie in $H^+ \cap B(\tau_0, R_c) \cap B(O, R_c) \setminus B(O, d_0)$ and n_2 must lie in $H^- \cap B(\tau_0, R_c) \cap B(O, R_c) \setminus B(O, d_0)$. In addition, considering the distance between n_1 and n_2 should be at most R_c and the origin should be inside the triangle

formed by τ_0 , n_1 and n_2 , n_1 must lie in the shadow area $A^+ = H^+ \cap B(\tau_0, R_c) \cap B(O, R_c) \setminus B(O, d_0) \cap B(M_2, R_c)$, shown in Figure 4. M_2 is one intersection point between the circle $C(O, d_0)$ and the circle $C(\tau_0, R_c)$, such intersection point must exist in this case since $R_c = \gamma R_s \leq 2R_s < 2d_0$.

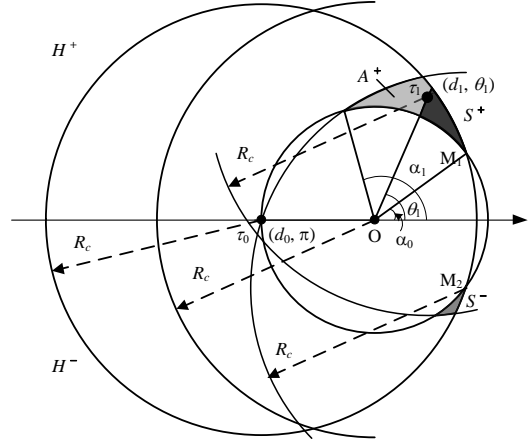


Fig. 4. Illustration of areas A^+ , S^+ and S^- in the case $\sqrt{3} < \gamma \leq 2$

Ordering the nodes in A^+ by increasing polar angle so that $\tau_1 = (d_1, \theta_1)$ has the smallest angle θ_1 . And assume the nodes τ_0 , τ_1 and another node $\tau_2 \in H^- \cap B(\tau_0, R_c) \cap B(O, R_c) \setminus B(O, d_0)$ can form a triangle which bounds a triangular hole containing the origin, then τ_2 must lie to the right of the line passing through τ_1 and O , denoted by $H^+(\theta_1)$ which contains all points with polar angle $\theta \in (\theta_1 - \pi, \theta_1)$. In addition, the distance to τ_1 is less than R_c . So the node τ_2 must lie in the region S^- , as illustrated in Figure 4.

$$S^-(\tau_0, \tau_1) = S^-(d_0, d_1, \theta_1) = H^- \cap B(\tau_0, R_c) \cap B(O, R_c) \setminus B(O, d_0) \cap H^+(\theta_1) \cap B(\tau_1, R_c)$$

Here we need to obtain the density of node τ_1 . Considering the way τ_1 was defined, there should be no nodes with a polar angle less than θ_1 , that is to say no nodes are in the region

$$S^+(\tau_0, \tau_1) = S^+(d_0, \theta_1) = A^+ \cap H^+(\theta_1)$$

Since the intensity measure of the Poisson process in polar coordinates is $\lambda r dr d\theta$, the density F_{τ_1} of τ_1 can be given as

$$F_{\tau_1}(dr_1, d\theta_1) = \lambda r_1 e^{-\lambda|S^+(d_0, \theta_1)|} dr_1 d\theta_1 \quad (7)$$

The integration domain $D(d_0)$ with respect to parameters (d_1, θ_1) can be easily obtained. From the construction of the area A^+ , we can get $\alpha_0 = 2 \arccos(R_c/(2d_0))$ and $\alpha_1 = 2 \arcsin(R_c/(2d_0)) - 2 \arccos(R_c/(2d_0))$. So $\alpha_0 \leq \theta_1 \leq \alpha_1$ and $d_0 < d_1 \leq R_1(d_0, \theta_1)$, where

$$R_1(d_0, \theta_1) = \min\left(\sqrt{R_c^2 - d_0^2 \sin^2 \theta_1} - d_0 \cos \theta_1, \sqrt{R_c^2 - d_0^2 \sin^2(\theta_1 + \alpha_0)} + d_0 \cos(\theta_1 + \alpha_0)\right)$$

Assume only τ_0, τ_1 and nodes in $S^-(\tau_0, \tau_1)$ can contribute to the triangle which bounds a triangular hole containing the origin, we can get a lower bound of the probability that the origin is inside a triangular hole. It is a lower bound because it is possible that τ_1 can not contribute to a triangle which bounds a triangular hole containing the origin, but some other nodes with higher polar angles in the area A^+ can contribute to such a triangle. For example, in Figure 5, if there is no node in S^- but there are some nodes in S'^- , then τ_1 can not contribute to any triangle which bounds a triangular hole containing the origin, but τ'_1 can form such a triangle with τ_0 and another node in S'^- . Based on the assumption, we have

$$\begin{aligned}
& \mathbb{P}\left\{ \bigcup_{\{n_1, n_2\} \subseteq \Phi'_{r_0}} T((r_0, \pi), n_1, n_2) \right\} \\
& > \mathbb{P}\left\{ \bigcup_{n_2 \subseteq \Phi'_{r_0} \cap S^-(\tau_0, \tau_1)} T((r_0, \pi), \tau_1, n_2) \right\} \\
& = \iint_{D(r_0)} \mathbb{P}\left\{ \bigcup_{\substack{n_2 \subseteq \Phi'_{r_0} \cap \\ S^-(\tau_0, r_1, \theta_1)}} T((r_0, \pi), (r_1, \theta_1), n_2) \right\} F_{\tau_1}(dr_1, d\theta_1) \\
& = \iint_{D(r_0)} \mathbb{P}\{\Phi'_{r_0}(S^-(r_0, r_1, \theta_1)) > 0\} F_{\tau_1}(dr_1, d\theta_1)
\end{aligned} \tag{8}$$

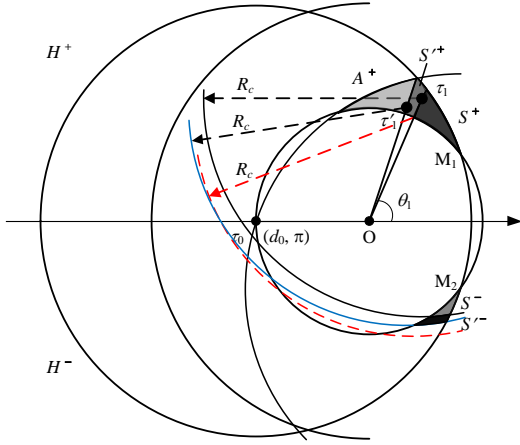


Fig. 5. Illustration of areas S'^+ and S'^- in the case $\sqrt{3} < \gamma \leq 2$

Therefore, from (5), (6), (7) and (8), the lower bound shown in (3) can be derived.

Next we will prove the upper bound. As discussed in Section IV.A, there are two cases for the origin being inside a triangular hole. As for the second case that the closest node τ_0 can not but some other nodes can contribute to a triangle which bounds a triangular hole containing the origin, it is not easy to obtain a closed-form expression for such probability, but we can get it by simulations. Simulation results show that this probability is less than 0.15% at any $\gamma \leq 3$ with any intensity λ . So we still focus on the probability of the first case.

For the lower bound, we only considered the case that τ_1 contributes to a triangle which bounds a triangular hole containing the origin. For the upper bound, we need to further

consider the case that τ_1 can not but some other nodes in A^+ can contribute to such a triangle, shown in Figure 5. Assume the node $\tau'_1 = (d'_1, \theta'_1)$ with the second smallest polar angle in A^+ can contribute to such a triangle, it means that there is no node in $S^-(d_0, d_1, \theta_1)$ but there is at least one node in the region $S'^-(d_0, d_1, \theta_1, d'_1, \theta'_1) = S^-(d_0, d'_1, \theta'_1) \setminus S^-(d_0, d_1, \theta_1)$.

Then the density of the pair (τ_1, τ'_1) is given as

$$\begin{aligned}
& F_{\tau_1, \tau'_1}(dr_1, d\theta_1, dr'_1, d\theta'_1) \\
& = \lambda^2 r_1 r'_1 e^{-\lambda |S^+(d_0, \theta'_1)|} dr_1 d\theta_1 dr'_1 d\theta'_1
\end{aligned} \tag{9}$$

The probability that τ_1 can not but τ'_1 can form a triangle which bounds a triangular hole containing the origin with τ_0 and another node in $S'^-(d_0, d_1, \theta_1, d'_1, \theta'_1)$ can be given as

$$\begin{aligned}
& \mathbb{P}\left\{ \bigcup_{\substack{\{n_2, n_3\} \subseteq \Phi'_{r_0} \cap \\ S^-(\tau_0, \tau'_1)}} T((r_0, \pi), \tau'_1, n_2) \mid T'((r_0, \pi), \tau_1, n_3) \right\} \\
& = \iiint \mathbb{P}\{\Phi'_{r_0}(S^-(r_0, r_1, \theta_1)) = 0\} \times \\
& \mathbb{P}\{\Phi'_{r_0}(S'^-(r_0, r_1, \theta_1, r'_1, \theta'_1)) > 0\} F_{\tau_1, \tau'_1}(dr_1, d\theta_1, dr'_1, d\theta'_1) \\
& = \iiint e^{-\lambda |S^-(r_0, r_1, \theta_1)|} \times \\
& (1 - e^{-\lambda |S'^-(r_0, r_1, \theta_1, r'_1, \theta'_1)|}) F_{\tau_1, \tau'_1}(dr_1, d\theta_1, dr'_1, d\theta'_1)
\end{aligned} \tag{10}$$

As we can see from Figure 5, as long as τ'_1 has a higher polar angle than τ_1 has, the sum of $|S^-(r_0, r'_1, \theta'_1)|$ and $|S'^-(r_0, r_1, \theta_1, r'_1, \theta'_1)|$ will be always smaller than $|S^-(r_0, r_0, \theta_1)|$.

Therefore we can get from (10)

$$\begin{aligned}
& \mathbb{P}\left\{ \bigcup_{\substack{\{n_2, n_3\} \subseteq \Phi'_{r_0} \cap \\ S^-(\tau_0, \tau'_1)}} T((r_0, \pi), \tau'_1, n_2) \mid T'((r_0, \pi), \tau_1, n_3) \right\} \\
& < \iiint (e^{-\lambda |S^-(r_0, r_1, \theta_1)|} e^{-\lambda |S^-(r_0, r_0, \theta_1)|}) \\
& F_{\tau_1, \tau'_1}(dr_1, d\theta_1, dr'_1, d\theta'_1)
\end{aligned} \tag{11}$$

Furthermore, let $S'^+(d_0, \theta_1, \theta'_1) = S^+(d_0, \theta'_1) \setminus S^+(d_0, \theta_1)$ then

$$\begin{aligned}
& \iint \lambda r'_1 e^{-\lambda |S'^+(d_0, \theta_1, \theta'_1)|} dr'_1 d\theta'_1 \\
& = 1 - e^{-\lambda |A^+ \setminus S^+(d_0, \theta_1)|} < 1
\end{aligned} \tag{12}$$

It is the complement of the probability that no node is in the area $A^+ \setminus S^+(d_0, \theta_1)$.

From (8), (9), (11) and (12), we can obtain

$$\begin{aligned}
& \mathbb{P}\left\{ \bigcup_{n_2 \subseteq \Phi'_{r_0} \cap S^-(\tau_0, \tau_1)} T((r_0, \pi), \tau_1, n_2) \right\} \\
& + \mathbb{P}\left\{ \bigcup_{\substack{\{n_2, n_3\} \subseteq \Phi'_{r_0} \cap \\ S^-(\tau_0, \tau'_1)}} T((r_0, \pi), \tau'_1, n_2) \mid T'((r_0, \pi), \tau_1, n_3) \right\} \\
& < \iint_{D(r_0)} (1 - e^{-\lambda |S^-(r_0, r_0, \theta_1)|}) F_{\tau_1}(dr_1, d\theta_1)
\end{aligned} \tag{13}$$

Similarly, we can further consider the case that neither of τ_1 and τ'_1 can contribute to a triangle which bounds a triangular hole containing the origin, but other nodes with even higher polar angle can contribute to such a triangle. In this way, we can get the same result as (13).

Therefore, it can be derived that

$$\begin{aligned} & \mathbb{P}\left\{ \bigcup_{\{n_1, n_2\} \subseteq \Phi'_{r_0}} T((r_0, \pi), n_1, n_2) \right\} \\ & < \iint_{D(r_0)} (1 - e^{-\lambda|S^-(r_0, r_0, \theta_1)|}) F_{\tau_1}(dr_1, d\theta_1) \end{aligned} \quad (14)$$

From (2), (5), (6), (7) and (14), the upper bound shown in (4) can be derived.

Here we need to compute the areas of $S^+(r_0, \theta_1)$, $S^-(r_0, r_1, \theta_1)$ and $S^-(r_0, r_0, \theta_1)$. In fact, the areas $|S^+(r_0, \theta_1)|$, $|S^-(r_0, r_1, \theta_1)|$ and $|S^-(r_0, r_0, \theta_1)|$ have very similar expressions. For example, the area $|S^+(r_0, \theta_1)|$ can be expressed as

$$\begin{aligned} |S^+(r_0, \theta_1)| &= \int_{\alpha_0}^{\theta_1} d\theta \int_{r_0}^{R_1(r_0, \theta_1)} r dr \\ &= \frac{1}{2} \int_{\alpha_0}^{\theta_1} R_1^2(r_0, \theta_1) d\theta - \frac{r_0^2}{2} (\theta_1 - \alpha_0) \end{aligned}$$

When $\theta_1 \leq \pi/2 - \arccos(R_c/(2r_0))$

$$|S^+(r_0, \theta_1)| = I(\theta_1) - I(\alpha_0)$$

where

$$\begin{aligned} I(\theta) &= \frac{r_0^2}{2} \sin \theta \cos \theta + \frac{R_c^2}{2} \theta - \frac{R_c^2}{2} \arcsin \frac{r_0 \sin \theta}{R_c} \\ &\quad - \frac{r_0}{2} \sin \theta \sqrt{R_c^2 - r_0^2 \sin^2 \theta} - \frac{r_0^2}{2} \theta \end{aligned}$$

When $\pi/2 - \arccos(R_c/(2r_0)) < \theta_1 \leq \alpha_1$

$$\begin{aligned} |S^+(r_0, \theta_1)| &= 2|S^+(r_0, \pi/2 - \arccos(R_c/(2r_0)))| \\ &\quad - |S^+(r_0, \pi - 2 \arccos(R_c/(2r_0)) - \theta_1)| \end{aligned}$$

Similarly, $|S^-(r_0, r_1, \theta_1)|$ and $|S^-(r_0, r_0, \theta_1)|$ can be obtained. ■

D. Case $\gamma > 2$

Theorem 3. When $\gamma > 2$, $p_l(\lambda, \gamma) < p(\lambda, \gamma) < p_u(\lambda, \gamma)$, where

$$\begin{aligned} p_l(\lambda, \gamma) &= 2\pi\lambda^2 \left\{ \int_{R_s}^{R_c/2} r_0 dr_0 \int_0^\pi d\theta_1 \int_{r_0}^{R'_1(r_0, \theta_1)} \right. \\ & e^{-\lambda\pi r_0^2} \times e^{-\lambda|S^+(r_0, \theta_1)|} (1 - e^{-\lambda|S^-(r_0, r_1, \theta_1)|}) r_1 dr_1 \\ & + \int_{R_c/2}^{R_c/\sqrt{3}} r_0 dr_0 \int_{\alpha_0}^{\alpha_1} d\theta_1 \int_{r_0}^{R_1(r_0, \theta_1)} e^{-\lambda\pi r_0^2} \\ & \left. \times e^{-\lambda|S^+(r_0, \theta_1)|} (1 - e^{-\lambda|S^-(r_0, r_1, \theta_1)|}) r_1 dr_1 \right\} \end{aligned} \quad (15)$$

and

$$\begin{aligned} p_u(\lambda, \gamma) &= 2\pi\lambda^2 \left\{ \int_{R_s}^{R_c/2} r_0 dr_0 \int_0^\pi d\theta_1 \int_{r_0}^{R'_1(r_0, \theta_1)} \right. \\ & e^{-\lambda\pi r_0^2} \times e^{-\lambda|S^+(r_0, \theta_1)|} (1 - e^{-\lambda|S^-(r_0, r_0, \theta_1)|}) r_1 dr_1 \\ & + \int_{R_c/2}^{R_c/\sqrt{3}} r_0 dr_0 \int_{\alpha_0}^{\alpha_1} d\theta_1 \int_{r_0}^{R_1(r_0, \theta_1)} e^{-\lambda\pi r_0^2} \\ & \left. \times e^{-\lambda|S^+(r_0, \theta_1)|} (1 - e^{-\lambda|S^-(r_0, r_0, \theta_1)|}) r_1 dr_1 \right\} \\ & + \mathbb{P}\left\{ \bigcup_{\{n_0, \dots, n_4\} \subseteq \Phi \setminus \{\tau_0(\Phi)\}} T(n_0, n_1, n_2) \mid T'(\tau_0, n_3, n_4) \right\} \end{aligned} \quad (16)$$

and

$$\begin{aligned} R'_1(r_0, \theta_1) &= \min\left(\sqrt{R_c^2 - r_0^2 \sin^2 \theta_1} - r_0 \cos \theta_1, \right. \\ & \left. \sqrt{R_c^2 - r_0^2 \sin^2 \theta_1} + r_0 \cos \theta_1\right) \end{aligned}$$

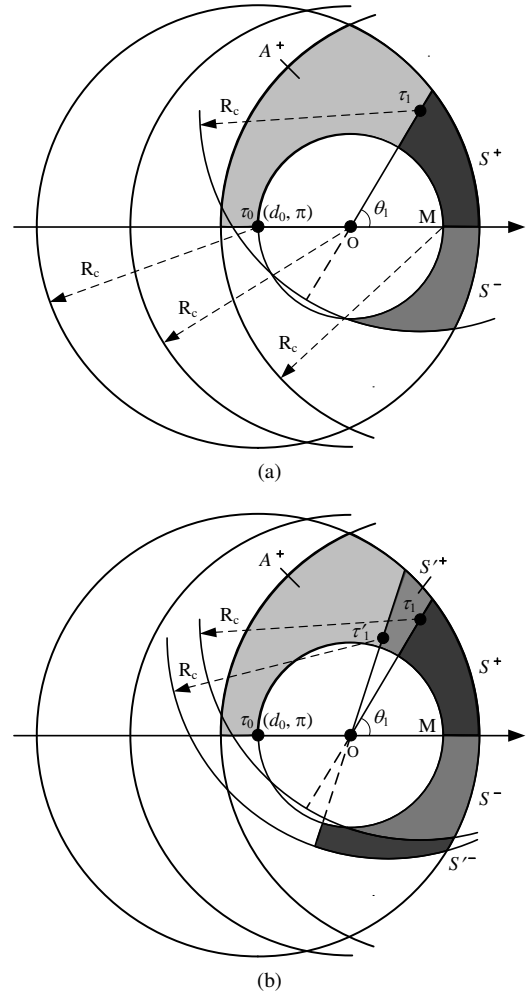


Fig. 6. Illustrations of areas in case $\gamma > 2$. (a) the areas A^+ , S^+ and S^- (b) the areas S'^+ and S'^-

In this case, we can use the same method as in Section IV.C to get the lower and upper bounds, shown in (15) and (16) respectively. But we need to consider two situations $R_s < d_0 \leq R_c/2$ and $R_c/2 < d_0 \leq R_c/\sqrt{3}$. In the first situation, $d_0 \leq R_c/2$ means that the ball $B(O, d_0)$ is included in the ball

$B(\tau_0, R_c)$. The illustrations for the areas A^+ , S^+ , S^- , S'^+ and S'^- are shown in Figure 6(a) and 6(b) respectively. In addition, the lower limit of integration for θ_1 is 0 and the upper limit is π . The second situation is the same as that in Section IV.C.

V. DISTRIBUTED COVERAGE HOLE DETECTION ALGORITHM

Our algorithm includes five components: weight computation, vertex and edge deletion, boundary edge detection, coarse boundary cycles discovery and boundary cycles minimization, as shown in Figure 7. An example is used to illustrate the procedures of this algorithm in Figure 8. For a WSN with some coverage holes, such as the one shown in Figure 8(a), our algorithm aims to discover minimum boundary cycles of all holes. In weight computation component, each node computes its weight independently. The definition of weight of a node will be presented in the next part. After obtaining the weight, each node continues to determine whether it can be deleted or not according to some rules defined hereafter. Figure 8(b) shows the result of vertex deletion. Furthermore, some special node will decide whether some edge can be deleted or not. Figure 8(c) shows the process of such special edge deletion. After the second component, many boundary edges can be found, as the red line shown in Figure 8(d). But it is possible that some other boundary edges have not been found. Then in the third component, all or nearly all boundary edges will be found after deleting some edges, see Figure 8(e-j). Then coarse boundary cycles can be easily discovered, as shown in Figure 8(k). It is possible that the found boundary cycles are not minimum. In this case, coarse boundary cycles will be minimized in the final component as shown in Figure 8(l).

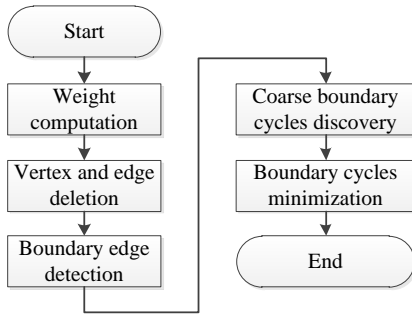


Fig. 7. Flow chart of the algorithm

A. Definitions

Before presenting the details of our algorithm, we first give some definitions that will be used in the process of the algorithm.

We say that a i -simplex $[v_{i0}, v_{i1}, \dots, v_{ii}]$ is part of a j -simplex $[v_{j0}, v_{j1}, \dots, v_{jj}]$ if $[v_{i0}, v_{i1}, \dots, v_{ii}] \subset [v_{j0}, v_{j1}, \dots, v_{jj}]$. So the vertex v_0 and v_1 is part of the edge v_0v_1 . The edge v_0v_1 is part of the triangle $v_0v_1v_2$. In addition, we use $E(v)$ to denote all the edges that the node v is part of and $T(v)$ to denote all the triangles that the node v is part of.

Definition 4 (Index of a triangle). *The index of a triangle Δ is the highest dimension of the simplex that the triangle is part of, denoted by I_Δ .*

Definition 5 (Weight of a node). *The weight of a fence node is defined to be 0. For any internal node v , if there exists one edge in $E(v)$ which is not part of any triangle, the weight w_v of node v is set to be 0; if not, the weight is the minimum index of all the triangles in $T(v)$, that is $w_v = \min_{\Delta \in T(v)} I_\Delta$.*

The weight of an internal node is an indicator of the density of surrounding nodes. If the weight of an internal node is 0, the node must be on the boundary of a coverage hole. The larger the weight is, the higher the probability that the node is not on the boundary of a coverage hole.

We also use the definition of simple-connectedness graph as in [27]. Let G be a simple graph with vertex set $V(G)$ and edge set $E(G)$. A cycle C is a sub-graph of G if it is connected and each vertex in C has degree two. The length of a cycle C is the number of its edges, denoted by $|E(C)|$. The cycle space $C(G)$ of a graph G contains all the cycles in G . The addition of two cycles C_1 and C_2 is defined as $C_1 \oplus C_2 = (E(C_1) \cup E(C_2)) \setminus E(C_1) \cap E(C_2)$. The triangle cycle subspace $C_T(G)$ of G is the set of all 3-length cycles in $C(G)$.

Definition 6 (Simple-Connectedness Graph). *A connected graph G is of simple connectedness if its cycle space $C(G)$ is empty, or for any cycle C in $C(G)$, there exists a set of 3-length cycles $T_0 \subseteq C_T(G)$ such that $C = \sum_{T \in T_0} T$.*

Let X be a vertex (or edge) set in a graph G , we use $G[X]$ to denote the vertex-induced (or edge-induced) sub-graph by X . The neighbour set of a vertex v in G is denoted by $N_G(v)$. The neighbouring graph $\Gamma_G(v)$ of vertex v is denoted as $G[N_G(v)]$. The neighbouring graph $\Gamma_G(e)$ of an edge $e = (u, v)$ is defined as $G[N_G(u) \cap N_G(v) \cup \{u, v\}] - e$. The neighbour set of k -simplex $[v_0, v_1, \dots, v_k]$ is defined as $\bigcap_{i=0}^k N_G(v_i)$.

Definition 7 (Deletion of k -simplex in Rips complex $\mathcal{R}(\mathcal{V})$). *A k -simplex $[v_0, v_1, \dots, v_k]$ is deleted in a Rips complex $\mathcal{R}(\mathcal{V})$ means that the simplex and all simplices which the simplex is part of are deleted from $\mathcal{R}_{R_c}(\mathcal{V})$.*

Based on definitions above, we can give the definition of HP (Homology Preserving) transformation.

Definition 8 (HP Transformation). *A HP transformation is a sequential combination of vertex (or edge) deletion as follows: a vertex (or edge) x of G is deletable if neighbouring graph $\Gamma_G(x)$ (1) has two or more vertices; (2) is connected and (3) is a simple-connectedness graph.*

Theorem 4. *HP transformations do not change the number of coverage holes in Rips complex of a WSN.*

Proof: In order to prove HP transformations do not change the number of coverage holes in Rips complex of a WSN, we only need to prove that in the process of any HP transformation, there is no new coverage holes created and no two coverage holes merged. If a new coverage hole is created when a vertex v (or edge e) is deleted, then the

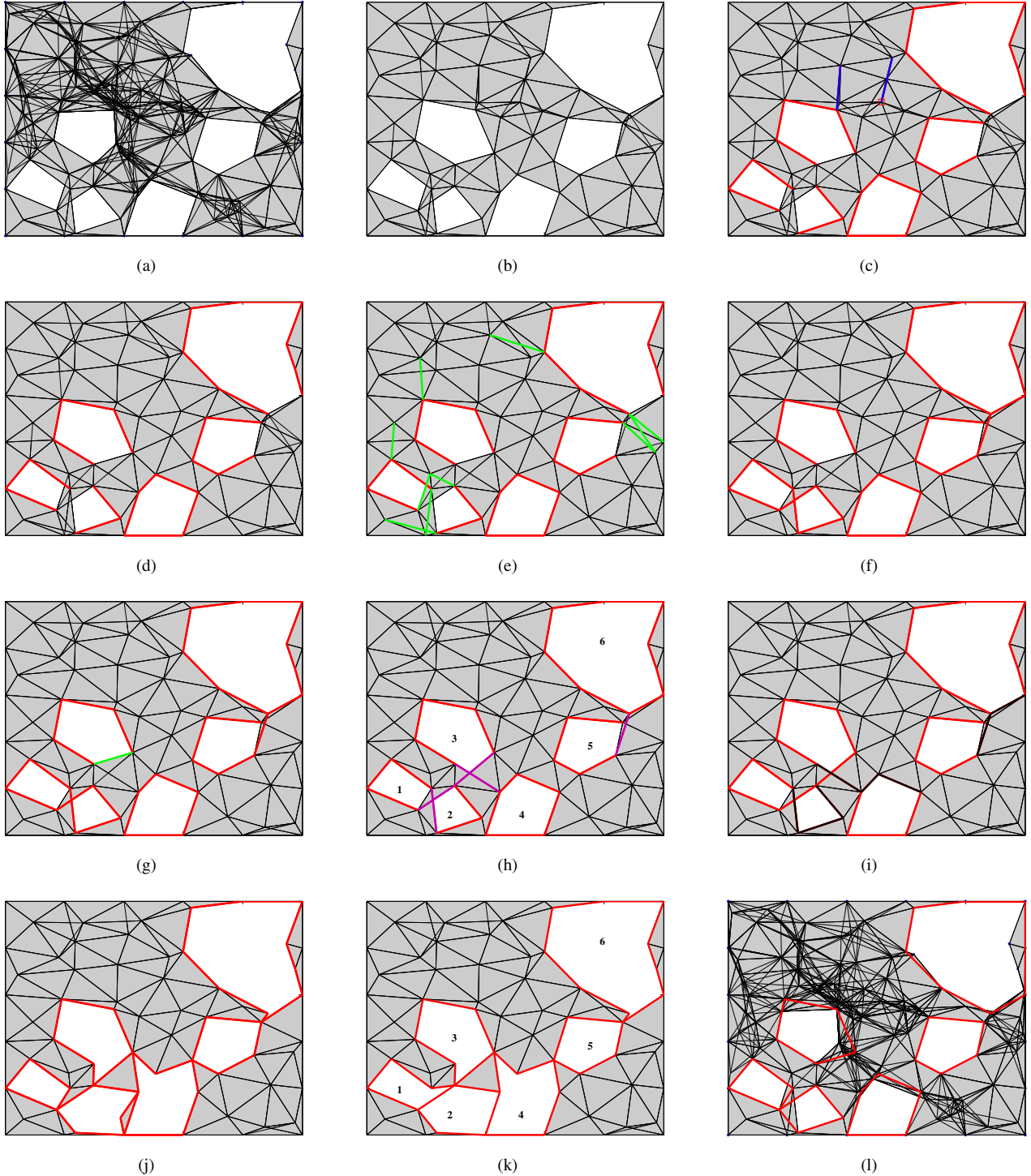


Fig. 8. Procedures of the boundary detection algorithm. (a) Rips complex of a WSN, (b) after vertex deletion, (c~d) edge deletion, (e~j) boundary edge detection, (k) coarse boundary cycles discovery, (l) boundary cycles minimization

boundary cycle of the new coverage hole must be a cycle in $\Gamma_G(v)$ (or $\Gamma_G(e)$), which means $\Gamma_G(v)$ is not a simple-connectedness graph. It is contrary to the third condition in HP transformation, so there is no new coverage hole created. Furthermore, if two coverage holes are merged when a vertex v (or edge e) is deleted, then the neighbour graph $\Gamma_G(v)$ ($\Gamma_G(e)$) must not be connected, which is contrary to the second condition in HP transformation. So no two coverage holes are

merged. Consequently, the number of coverage holes will not be changed in the process of any HP transformation. ■

B. Weight computation

In this component, each node computes its weight. For any fence node, its weight is 0. For any internal node, theoretically it needs to construct all the simplice it is part of. As we

consider WSNs in a planar target field, each internal node only needs to construct all its 1-simplex and 2-simplex and their neighbours. This can also reduce the computation complexity. In order to do this, the node needs to obtain all its 1- and 2-hop neighbours information. This can be easily achieved by two broadcasts of hello message. In the first one, each node broadcasts its id. When it gets all the ids of its 1-hop neighbours, each node continues to broadcast a hello message containing the ids of its 1-hop neighbours. After receiving the neighbour list of its neighbours, the node can obtain its $E(v)$, the set of edges (1-simplex) and $T(v)$, the set of triangles (2-simplex). It can also get the neighbours of each simplex. For any $e \in E(v)$, let $n(e)$ denote the neighbour set of e . For any $t \in T(v)$, let $n(t)$ denote the neighbour set of t . Then the weight of node v can be computed as in Algorithm 1.

Algorithm 1 Weight computation (for internal node v)

Begin

```

if  $\exists e \in E(v), n(e)$  is empty then
   $w_v = 0$ 
else if  $\exists t \in T(v), n(t)$  is empty then
   $w_v = 2$ 
else
   $w_v = 3$ 
end if

```

END

C. Vertex and edge deletion

In this component, we conduct maximal vertex deletion without changing the number of coverage holes in the original WSN and also delete some special edges if such edges exist.

1) *Vertex deletion*: From the definition of weight, we can see that the higher the weight is, the higher is the probability that the sensing range of the node is fully covered by its neighbours, consequently the probability that the node does not lie on the boundary is higher. Meanwhile, if the deletion of a vertex may create a new coverage hole, it must not be deleted no matter how high the weight is. So we have such a rule for vertex deletion. If the weight of a vertex is smaller than 3, it should never be deleted. Otherwise, the vertex continues to check whether it is deletable or not according to HP transformation. After the verification, the vertex broadcasts a message indicating that it can be deleted or not. After receiving the status of all its neighbours, each deletable vertex continues to check whether it should be deleted. It can be found that the weight of any deletable vertex must be 3. We assume that the vertex with lower ID has the priority to be deleted first. So each deletable vertex just needs to check whether its ID is the lowest among all its deletable neighbours. If so, it should be deleted. Otherwise, it should not be deleted. Algorithm 2 gives the detailed process for vertex deletion. According to the rule, it can be seen that two neighbouring vertices will not be deleted simultaneously, so each vertex can make the decision independently. When a vertex is deleted, it broadcasts a message to its neighbours. All its neighbours will modify their simplices accordingly and compute their weights again.

The procedure of vertex deletion terminates until no vertex can be deleted in the Rips complex. Figure 8(b) gives the final result after vertex deletion.

Algorithm 2 Vertex deletion (for internal node v)

Begin

```

if  $w_v < 3$  then
  node  $v$  can not be deleted
else if node  $v$  is not deletable according to HP transformation then
  node  $v$  can not be deleted
else if the ID of node  $v$  is the smallest among all its deletable neighbours then
  node  $v$  is deleted
end if

```

END

2) *Edge deletion*: After vertex deletion, we find one interesting thing. It is highly possible that an edge having only one neighbour lies on the boundary of a coverage hole, such as the red edges shown in Figure 8(c). It is also possible that there exist some special such edges not lying on the boundary, such as the blue edges shown in Figure 8(c). We try to delete such special edges. Since the edge has only one neighbour, deleting the edge will not change the number of coverage holes. We design a rule for edge deletion. If a vertex has only one special edge and deletion of the special edge can make the vertex have a Hamilton cycle in its left neighbouring graph, then such a special edge can be deleted. According to this rule, nearly all edges which have only one neighbour and are not lying on the boundary of any holes can be deleted. But it is also possible that some such edges lying on the boundary are also deleted. This is not a big issue, because deletion of such edges will not change the number of coverage holes and just enlarge the current coverage holes. It can be solved in the boundary cycles minimization component. In addition, after edge deletion, it is possible that some vertices can be deleted again, such as the vertex denoted by red square in Figure 8(c). If such a case happens, we can continue to do vertex deletion until no more vertex or edge can be deleted. Figure 8(d) shows the result after edge deletion. Here we need to talk a little more about Hamilton cycle. In general, it is a NP-complete problem to find a Hamilton cycle in a graph. However, considering the left nodes after vertex deletion usually have very small number of neighbouring nodes, it is not complicated to check the existence of a Hamilton cycle in their neighbouring graph even if we use exhaustive search method.

D. Boundary edge detection

After deleting some vertices and edges, we continue to look for the edges which have only one neighbour. It can be seen that nearly all such edges lie on the boundary of holes. We call them boundary edges. It can also be found that some edges lying on the boundary have not been found. In this component, we try to find such edges as many as possible. In all cases, such edges have two or more neighbours. If we consider the nodes having one or more boundary edges as

boundary nodes and other nodes as non-boundary nodes, then we try to delete some edges connecting non-boundary nodes and boundary nodes according to HP transformation, such as the green edges shown in Figure 8(e). After that, it is possible that some new boundary edges are recognized as shown in Figure 8(f). And it is also possible that some edges lying on the boundary have still not been discovered. Such case usually occurs when some boundary nodes are neighbours and edges connecting them have more than one neighbours. In this case, we randomly delete some of such edges according to HP transformation, such as the green edges in Figure 8(g). After that, some new boundary edges can be recognized, as shown in Figure 8(h).

But it is possible that the new found boundary edges are not correct, as the magenta edge in coverage hole 5 in Figure 8(h), or can not construct a cycle with other boundary edges, as the magenta edges in coverage hole 1, 2 and 3 in Figure 8(h). As for the case in coverage hole 5, we define such a rule to delete a boundary edge. For any internal node v , if it has two boundary neighbour nodes u and w , the edge vu and vw are not boundary edge and wu is a boundary edge, if the deletion of the edge wu can make at least one of the two edges vu and vw be boundary edge, then wu can be deleted. As for the case in coverage holes 1, 2 and 3, it is often due to the fact that two boundary edges cross with each other. It is found from numerous simulations that there are mainly three cases of crossing boundary edges, as shown in Figure 9, red lines denote boundary edges and black ones denote non-boundary edges. Similarly, we define some rules to delete such edges. We still take node v as an example, in the top part of Figure 9(a), the two red lines connecting v and its neighbours are deleted, as shown in the bottom part of Figure 9(a). For the cases in Figure 9(b) and (c), the red line connecting v and its neighbour is deleted, as shown in the bottom part of Figure 9(b) and (c). According to such rules, some boundary edges can be deleted, such as the black bold edges in Figure 8(i). From Figure 8(i), it can be found that certain boundary edge is deleted incorrectly. It is not a big issue as explained in last part. Deleting such edges will not change the number of coverage holes and just enlarge the current holes, it will be solved in the process of minimizing boundary cycles. After deletion of such edges, new boundary edges can be found as shown in Figure 8(j).

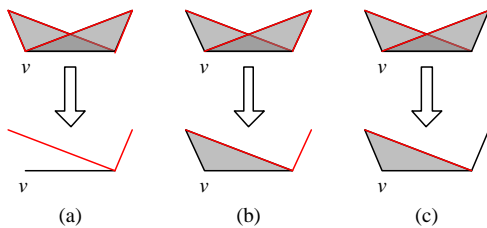


Fig. 9. Illustration of crossing boundary edges

In general, after the process above, nearly all boundary edges can be found. But there exists one special case as in Figure 10. In this case, some edges lying on the boundary can not be detected. It can be solved in the next component.

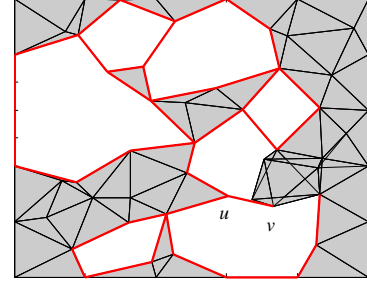


Fig. 10. Special case when some boundary edges can not be detected

E. Coarse boundary cycles discovery

After boundary edges are detected in the former component, it is easy to discover the coarse boundary cycles. We just need to randomly choose one node which has two boundary edges in any boundary cycle. The node initiates the process to find the coarse boundary cycle by sending a message along one of the boundary edges. Then the boundary neighbour continues sending the message along its boundary edges. When the initiating node receives the message coming back along the other boundary edge, it discovers one coarse boundary cycle. Similarly, all coarse boundary cycles can be found, as shown in Figure 8(k).

As for the special case shown in Figure 10, when the node v receives a message from its boundary neighbour node u , it broadcasts the message to all its neighbours except u . If its neighbour node is a boundary node, then the message can be sent along the boundary edges. If its neighbour node is not a boundary node but it has boundary neighbour nodes, then it can send the message to its boundary neighbour nodes. Else, it will not transmit the message again. In this way, the message goes along boundary edges most of the time and can return to the original node initiating the message.

F. Boundary cycles minimization

It is possible that some primary boundary cycles found are not minimum, so we need to minimize such cycles. This can be achieved by checking whether there exists shorter path between any two nodes in the cycle. Since each node has its 1- and 2-hop neighbours information, it can locally check the existence of shorter path in the cycle in general cases. If there exists, we shorten the cycle and continue to do the same verification until no such case exists. After that, it is still possible some cycle has not been minimized, such as the coverage hole 2 in Figure 8(k). So we use the following 2-hop shrinking process to make the cycle as shorter as possible. For any four adjacent nodes in the cycle, say a, b, c, d , if there exists one node x which is one common neighbour of nodes a, b, c, d , then the cycle can be shortened by using x to replace nodes b and c .

In this way, we can nearly obtain most minimum cycles surrounding coverage holes. It is also possible that in some cases, we can not get the minimum cycles since each node only has its 1- and 2-hop neighbours information. Even so, the boundary cycles discovered in the algorithm can still provide

valuable information about coverage holes. Theoretically, if each node has more information about its k -hop neighbours, all cycles can be minimized.

VI. SIMULATIONS AND PERFORMANCE EVALUATION

Performance evaluation of the theoretical bounds obtained in Section IV and the algorithm proposed in Section V is presented in this section.

A. Simulation settings

We have different simulation settings to evaluate the bounds and the algorithm.

For bounds evaluation, a disk centered at the origin with radius R_c is considered in the simulations. The probability that the origin is inside a triangular hole is computed. Sensors are randomly distributed in the disk according to a Poisson point process with intensity λ . The sensing radius R_s of each node is set to be 10 meters and γ is chosen from 2 to 3 with interval of 0.2. So the communication radius R_c ranges from 20 to 30 meters with interval of 2 meters. λ is selected from 0.001 to 0.020 with interval of 0.001. For each γ , 10^7 simulations are run under each λ to check whether the origin belongs to a triangular hole.

For performance evaluation of the algorithm, we choose a 100×100 m² square area as the target field. The sensing radius R_s of each node is 10 meters. The communication radius R_c is set to be 20 meters and so $\gamma = 2$. There are fence sensors locating along the edges of the square with 20 meters distance between neighbours. Other internal sensors are randomly distributed in the area according to a Poisson point process with intensity λ .

B. Proportion of the area of triangular holes

The probability $p(\lambda, \gamma)$ obtained by simulation is presented with the lower and upper bounds in Figure 11(a) and 11(b) respectively. It can be seen that for any value of γ , $p(\lambda, \gamma)$ has a maximum at a threshold value λ_c of the intensity.

As a matter of fact, for $\lambda \leq \lambda_c$, the number of nodes is small. Consequently the probability that the origin belongs to a triangular hole is relatively small too. With the increase of λ , the connectivity between nodes becomes stronger. As a result, the probability that the origin belongs to a triangular hole increases. However, when the intensity reaches the threshold value, the origin is covered with maximum probability. $p(\lambda, \gamma)$ decreases for $\lambda \geq \lambda_c$. The simulations also show that λ_c decreases with the increase of γ .

On the other hand, it can be seen from Figure 11(a) and 11(b) that for a fixed intensity λ , $p(\lambda, \gamma)$ increases with the increases of γ . That is because when R_s is fixed, the larger R_c is, the higher is the probability of each triangle containing a coverage hole.

Furthermore, the maximum probability increases quickly with γ ranging from 2.0 to 3.0. It is shown that when $\gamma = 2$, the maximum probability from simulation is about 0.03% and thus it is acceptable to use Rips complex based algorithms to discover coverage holes. While the ratio γ is high to a certain

extent, it is unacceptable to use connectivity information only to discover coverage holes.

Finally, it can be found in Figure 11(a) that the probability obtained by simulation is very well consistent with the lower bound. The maximum difference between them is about 0.5%. Figure 11(b) shows that probability obtained by simulation is also consistent with the upper bound. The maximum difference between them is about 3%.

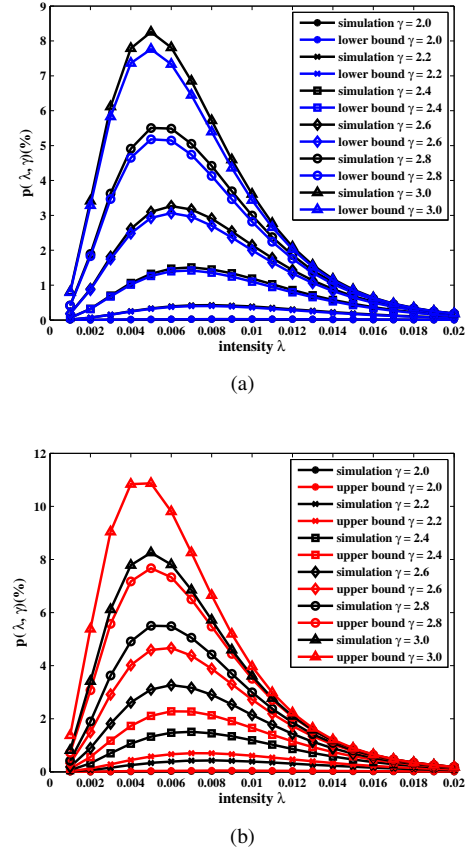


Fig. 11. Proportion of the area of triangular holes (a) simulation results and lower bounds ; (b) simulation results and upper bounds

C. Performance of the algorithm

1) *Complexity*: The computation complexity of each step in the algorithm is shown in Table I. In the weight computation component, each node only needs to check all its 2-simplex, so the computation complexity is $O(n^2)$, where n is the number of its 1-hop neighbours.

In vertex deletion part, each node needs to check whether it is deletable or not according to HP transformation. This can be done by checking all its cycles in its neighbouring graph. It can build a spanning tree in its neighbouring graph and check all fundamental cycles in the spanning tree. There are $E - n + 1$ fundamental cycles, where E is the number of edges in its neighbouring graph, so the worst case computation complexity is $O(n^2)$. Since the node needs to recompute its weight and recheck whether it is deletable when any one of its neighbour is deleted, so the total worst case computation complexity is $O(n^3)$. As for the edge deletion, only limited

TABLE I
COMPLEXITY OF EACH STEP IN THE ALGORITHM

Step	Complexity
Weight computation	$O(n^2)$
Vertex and edge deletion	$O(n^3)$
Boundary edge detection	$O(n^3)$
Coarse boundary cycles discovery	$O(1)$
Boundary cycles minimization	$O(1)$

nodes will do this process and the complexity is not high as explained in Section V.C.

In the boundary edge detection component, the non-boundary nodes need to check whether the edge connecting itself with its boundary neighbours can be deleted or not according to HP transformation. So the worst case computation complexity is $O(n^3)$, the actual complexity is much less than that since for one edge, there are usually very few nodes in its neighbouring graph. The boundary nodes also need to check whether the edges connecting itself and its boundary neighbours can be deleted or not, so the complexity is also $O(n^3)$. In addition, the boundary nodes need to check whether there exist special cases as illustrated in Section V.D. The worst case computation complexity for such process is $O(n^2)$. So the complexity of this step is $O(n^3)$.

As for the final two components, each node only needs to broadcast some messages and do some local computations, the complexity is $O(1)$. So the total worst case computation complexity for our algorithm is $O(n^3)$.

2) *Comparison with other algorithms*: In order to evaluate the performance of our proposed homology based algorithm (denoted as HBA), we compare it with the location based algorithm (denoted as LBA) proposed in [19]. Since location based algorithm can discover both triangular and non-triangular coverage holes, but our algorithm can only detect non-triangular coverage holes, we do not consider those triangular coverage holes in the comparison. Since it is possible that there exist shorter paths in boundary cycles found by LBA, we first shrink them using 1-hop neighbour information of boundary nodes. After that, we compare those boundary cycles with what our algorithm finds. Since for some coverage holes, the minimum boundary cycles may not be unique, two boundary cycles are considered to surround the same coverage hole if one cycle can be converted to another one by using only 1-hop neighbours information. We emphasize that only 1-hop neighbours information can be used in the comparison in order to evaluate the accuracy of boundary cycles found by our algorithm. For example, if one cycle c_1 found by our algorithm can not be converted to another cycle c_2 found by LBA using only 1-hop neighbours information but can be converted by using 2-hop neighbours information, we consider the cycle c_1 is not accurate and the corresponding coverage hole is not found.

Based on the method presented above, we set λ to be 0.008, 0.010 and 0.012 to represent sparse, moderate and dense WSNs respectively. For each intensity, 1000 simulations are performed. Simulation results show that when λ is 0.008, there are nine times among the 1000 times when our algorithm can not find all non-triangular coverage holes. In each of the nine

times, only one coverage hole is missed. There are 7363 non-triangular holes in total and 7354 ones found by our algorithm. When λ is 0.010 and 0.012, only one time among the 1000 times when our algorithm can not find all coverage holes. And in that time, only one coverage hole is missed. When λ is 0.010, there are 6114 non-triangular holes in total and 6113 ones found by our algorithm. When λ is 0.012, there are 4613 non-triangular holes in total, of which 4612 ones are found. The results are shown in Figure 12. All these results show that our algorithm can find about 99% coverage holes in about 99% cases.

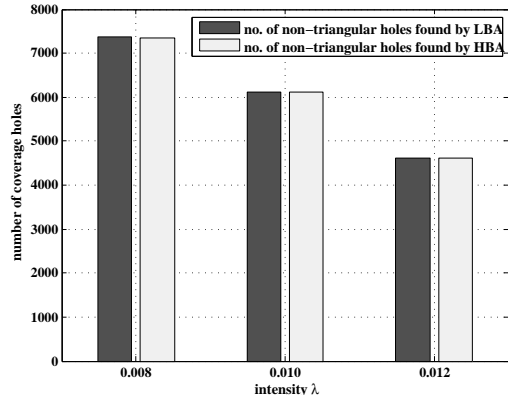


Fig. 12. Performance evaluation of the algorithm

VII. CONCLUSIONS

In this paper, we adopt two types of simplicial complex called Čech complex and Rips complex to capture coverage holes of a WSN. The relationship between Čech complex and Rips complex in terms of coverage hole is first analysed under different ratios between communication radius and sensing radius of a sensor. Based on that, we define two types of coverage holes: triangular and non-triangular hole. For triangular holes, both the lower and upper bounds on the proportion of the area of triangular holes in a WSN are derived. Such proportion is related to the ratio between communication radius and sensing radius of each sensor. When the ratio is no larger than $\sqrt{3}$, there is no triangular hole. When the ratio is between $\sqrt{3}$ and 2, both the theoretical analysis and simulation results show that the proportion is lower than 0.06% under any intensity. It means that the triangular holes can nearly be neglected. When the ratio is larger than 2, the proportion of the area of triangular holes increases with γ . It becomes unacceptable for γ larger than a threshold. In that case triangular holes can not be neglected any more. For non-triangular holes, a homology-based algorithm is proposed to detect them. Simulation results show that the algorithm can detect 99% such holes.

REFERENCES

- [1] Q. Fang, J. Gao, and L. Guibas, "Locating and bypassing routing holes in sensor networks," in *Proc. IEEE INFOCOM*, vol. 4, Mar. 2004, pp. 2458–2468.

- [2] G. Wang, G. Cao, and T. La Porta, "Movement-assisted sensor deployment," in *Proc. IEEE INFOCOM*, vol. 4, Mar. 2004, pp. 2469–2479.
- [3] C. Zhang, Y. Zhang, and Y. Fang, "Localized algorithms for coverage boundary detection in wireless sensor networks," *Wirel. Netw.*, vol. 15, no. 1, pp. 3–20, Jan. 2009.
- [4] —, "Detecting coverage boundary nodes in wireless sensor networks," in *Proc. IEEE International Conference on Networking, Sensing and Control*, Ft. Lauderdale, Florida, USA, Apr. 2006, pp. 868–873.
- [5] Y. Bejerano, "Simple and efficient k-coverage verification without location information," in *Proc. IEEE INFOCOM*, Phoenix, Arizona, USA, Apr. 2008, pp. 897–905.
- [6] —, "Coverage verification without location information," *IEEE Trans. Mobile Comput.*, vol. 11, no. 4, pp. 631–643, Apr. 2012.
- [7] V. de Silva, R. Ghrist, and A. Muhammad, "Blind swarms for coverage in 2-d," in *Proc. Robotics: Science and Systems*, Cambridge, MA, Jun. 2005, pp. 335–342.
- [8] V. de Silva and R. Ghrist, "Coverage in sensor networks via persistent homology," *Algebraic & Geometric Topology*, vol. 7, pp. 339–358, 2007.
- [9] R. Ghrist and A. Muhammad, "Coverage and hole-detection in sensor networks via homology," in *Proc. 4th International Conference on Information Processing in Sensor Networks*, Los Angeles, California, USA, Apr. 2005, pp. 254–260.
- [10] A. Muhammad and M. Egerstedt, "Control using higher order laplacians in network topologies," in *Proc. 17th International Symposium on Mathematical Theory of Networks and Systems*, Kyoto, Japan, Jul. 2006, pp. 1024–1038.
- [11] A. Tahbaz-Salehi and A. Jadbabaie, "Distributed coverage verification in sensor networks without location information," *IEEE Trans. Autom. Control*, vol. 55, no. 8, pp. 1837–1849, Aug. 2010.
- [12] B. Liu and D. Towsley, "A study of the coverage of large-scale sensor networks," in *Proc. IEEE MASS*, Fort Lauderdale, Florida, USA, Oct. 2004, pp. 475–483.
- [13] L. Lazos and R. Poovendran, "Stochastic coverage in heterogeneous sensor networks," *ACM Trans. Sen. Netw.*, vol. 2, no. 3, pp. 325–358, Aug. 2006.
- [14] P.-J. Wan and C.-W. Yi, "Coverage by randomly deployed wireless sensor networks," *IEEE Trans. Inf. Theory*, vol. 52, no. 6, pp. 2658–2669, Jun. 2006.
- [15] X. Li, D. K. Hunter, and S. Zuyev, "Coverage properties of the target area in wireless sensor networks," *IEEE Trans. Inf. Theory*, vol. 58, no. 1, pp. 430–437, Jan. 2012.
- [16] F. Yan, P. Martins, and L. Decreusefond, "Accuracy of homology based approaches for coverage hole detection in wireless sensor networks," in *Proc. IEEE ICC*, Ottawa, Canada, Jun. 2012.
- [17] C. Huang and Y. Tseng, "The coverage problem in a wireless sensor network," in *Proc. ACM WSN*, San Diego, California, USA, Sep. 2003, pp. 115–121.
- [18] X. Wang, G. Xing, Y. Zhang, C. Lu, R. Pless, and C. Gill, "Integrated coverage and connectivity configuration in wireless sensor networks," in *Proc. ACM SenSys*, Los Angeles, CA, USA, Nov. 2003, pp. 28–39.
- [19] B. Tong and W. Tavanapong, "On discovering sensing coverage holes in large-scale sensor networks," Computer Science, Iowa State University, Tech. Rep. TR 06-03, Mar. 2006.
- [20] A. Muhammad and A. Jadbabaie, "Decentralized computation of homology groups in networks by gossip," in *Proc. American Control Conference*, New York, NY, USA, Jul. 2007, pp. 3438–3443.
- [21] S. Funke, "Topological hole detection in wireless sensor networks and its applications," in *Proc. joint workshop on Foundations of mobile computing*, Cologne, Germany, Sep. 2005, pp. 44–53.
- [22] S. Funke and C. Klein, "Hole detection or: how much geometry hides in connectivity?" in *Proc. 22nd annual symposium on Computational geometry*, Sedona, Arizona, USA, Jun. 2006, pp. 377–385.
- [23] A. Kroller, S. P. Fekete, D. Pfisterer, and S. Fischer, "Deterministic boundary recognition and topology extraction for large sensor networks," in *Proc. ACM SODA*, Miami, Florida, USA, Jan. 2006, pp. 1000–1009.
- [24] Y. Wang, J. Gao, and J. S. Mitchell, "Boundary recognition in sensor networks by topological methods," in *Proc. ACM MobiCom*, Los Angeles, California, USA, Sep. 2006, pp. 122–133.
- [25] D. Dong, Y. Liu, K. Liu, and X. Liao, "Distributed coverage in wireless ad hoc and sensor networks by topological graph approaches," in *Proc. IEEE ICDCS*, Genova, Italy, Jun. 2010, pp. 106–115.
- [26] H. Zhou, S. Xia, M. Jin, and H. Wu, "Localized algorithm for precise boundary detection in 3d wireless networks," in *Proc. IEEE ICDCS*, Genova, Italy, Jun. 2010, pp. 744–753.
- [27] D. Dong, Y. Liu, and X. Liao, "Fine-grained boundary recognition in wireless ad hoc and sensor networks by topological methods," in *Proc. ACM MobiHoc*, New Orleans, Louisiana, USA, May 2009, pp. 135–144.

- [28] M. A. Armstrong, *Basic Topology*. Springer, 1983.
- [29] J. Munkres, *Elements of algebraic topology*. Addison-Wesley, 1984.
- [30] A. Hatcher, *Algebraic Topology*. Cambridge University Press, 2002.
- [31] G. S. Kasbekar, Y. Bejerano, and S. Sarkar, "Lifetime and coverage guarantees through distributed coordinate-free sensor activation," in *Proc. ACM MobiCom*, Beijing, China, Sep. 2009, pp. 169–180.
- [32] C. Bettstetter and J. Zangl, "How to achieve a connected ad hoc network with homogeneous range assignment: an analytical study with consideration of border effects," in *Proc. 4th International Workshop on Mobile and Wireless Communications Network*, Stockholm, Sweden, Sep. 2002, pp. 125–129.



Feng Yan received the B.S. degree from Huazhong University of Science and Technology, China, in 2005 and the M.S. degree from Southeast University, China, in 2008, both in electrical engineering. He is currently pursuing the Ph.D degree in the Network and Computer Science Department, at Telecom ParisTech, Paris, France. His current research interests are in the areas of wireless communications and wireless networks, with emphasis on applications of homology theory in wireless networks.

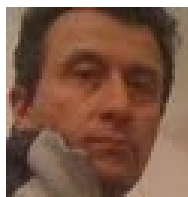


Anais Vergne received the M.S. degree in telecommunications from Telecom ParisTech, Paris, France in 2010. She is currently working towards the Ph.D. degree in the Network and Computer Science department, at Telecom ParisTech. Her research interests include stochastic geometry applications to wireless networks, more particularly algebraic topology applied to wireless sensor networks.



Philippe Martins received a M.S. degree in signal processing and another M.S. degree in networking and computer science from Orsay University and ESIGETEL France, in 1996. He received the Ph.D. degree with honors in electrical engineering from Telecom ParisTech, Paris, France, in 2000.

He is currently a Professor in the Network and Computer Science Department, at Telecom ParisTech. His main research interests lie in performance evaluation in wireless networks (RRM, scheduling, handover algorithms, radio metrology). His current investigations address mainly three issues: a) the design of distributed sensing algorithms for cognitive radio b) distributed coverage holes detection in wireless sensor networks c) the definition of analytical models for the planning and the dimensioning of cellular systems. He has published several papers on different international journals and conferences. He is also an IEEE senior member and he is co-author of several books on 3G and 4G systems.



Laurent Decreusefond is a former student of Ecole Normale Supérieure de Cachan. He obtained his Ph.D. degree in Mathematics in 1994 from Telecom ParisTech and his Habilitation in 2001. He is currently a Professor in the Network and Computer Science Department, at Telecom ParisTech. His main fields of interest are the Malliavin calculus, the stochastic analysis of long range dependent processes, random geometry and topology and their applications. With P. Moyâl, he co-authored a book about the stochastic modelling of telecommunication

systems.